RSC Advances

ROYAL SOCIETY OF CHEMISTRY

www.rsc.org/advances

The influence of aluminum chloride on biosynthetic Schwertmannite and the Cu(II)/Cr(VI) adsorption

Min Gan[a], Zhihe Zheng[a], Shengjie Sun[a], Jianyu Zhu[a]*, Xinxing Liu[a]

[a]*School of Minerals Processing and Bioengineering, Key Laboratory of Biometallurgy of Ministry of Education, Central South University, Changsha 410083, China;*

***Corresponding authors:**

Jianyu Zhu, E-mail: zhujy@mail.csu.edu.cn

School of Minerals Processing and Bioengineering, Key Laboratory of Biometallurgy of Ministry of Education, Central South University, Changsha 410083, China

Tel: +86-731- 88836944

ABSTRACT

Iron oxyhydroxides Schwertmannite and Akaganèite are recognized as promising absorbent in the heavy metal contaminated water treatment. In this study, aluminium chloride modified Schwertmannite was biosynthesized by *Acidithiobacillus ferrooxidans* and characterized by SEM, FTIR, XRD, TGA, potentiometric titrations and XPS. The effect of pH, adsorption kinetic, isotherm and mechanism were systematic investigated. With aluminium chloride increasing, the adsorbent transformed from nanoscale villus covered spherical aggregates to rodlike structure consisting globe, and facilitated the crystallinity decreasing and akaganèite formation. The optimum pH for Cr(VI) adsorption was maintained between 6.0-7.0, while the Cu(II) adsorption was increased over pH range 4.0-8.0. Adsorption kinetic varied with pH and adsorbents. The equilibrium reached within 30 min for both metals, and the pseudo-second-order model well fitted the adsorption process. The maximum Cu(II) and Cr(VI) adsorption reached 23.95 and 57.60 mg/g which occurred in $FeSO_4 \cdot 7H_2O/AlCl_3$ ratio in 15:5 and 15:10 respectively. As for the binary metals system, the maximum adsorption for Cu(II) and Cr(VI) was 14.10 and 28.89 mg/g, achieved with $FeSO_4.7H_2O/AlCl_3$ ratio in 15:5. The modification enhanced the adsorption capacity effectively. Additionally, the adsorbent could be effectively regenerated through pH 2.0 water washing. FTIR, XPS and released proton correlation analysis revealed that –O-H, O-H-Cl and SO_4^{2-} were the key groups in adsorption. Heavy metals adsorbed on Schwertmannite through anion-exchange and surface complexation. Heavy metals can be efficient removed by the modified biosynthetic Schwertmannite.

Keywords: *Acidithiobacillus ferrooxidans*, Schwertmannite, Modification, Adsorption, Chromium/Copper

1. Introduction

Heavy metals have posed significant threat to the environment and public health because of their acute toxicity, non-biodegradable nature and tendency for bioaccumulation[1-3]. They usually discharge into the natural environment in anthropogenic activities without sufficient treatment. Among the toxic heavy metals, Cu(II) and Cr(VI) are considered as two priority pollutants. The upper limitation of Cu(II) and Cr(VI) in drinking water was set at 1.3 and 0.1 mg/L respectively by the World Health Organization.[1] It was an urgent and challenge issue to removal heavy metals from contaminated water.

Various techniques such as chemical precipitation, membrane filtration, coagulation, and ion exchange have been applied in water treatment area. While the limitation such as poor performance to low concentration metals, high cost and lack of selectivity made most of these processes impractical. Adsorption has attracted increasing interest due to its simplicity, convenience, and high removal efficiency.[4, 5] It offers flexibility in design and operation, and it generates high-quality treated effluent.[6, 7] The key to the adsorption techniques depends on the efficient adsorbent, which requires the adsorbent possessing high surface area and strong affinity.[8, 9] Among the widely used adsorbents, metal oxides, such as nanosized ferric oxides, aluminum oxides, manganese oxides, are considered as the promising ones for heavy metals removal.[6, 10] The huge reserve, facile in synthesis, and environmental friendliness made the iron based adsorption materials to be the most widely used adsorbent. The previous study about ferric oxide mainly concentrated on chemical synthetic goethite, hematite, amorphous hydrous, maghemite and magnetite, etc.[11,12] In recent years, iron oxyhydrosulfate has gained increasing attention in geological, environmental and metallurgical fields because of the high specific surface area, reactivity and tunnel structure.

Schwertmannite is a poorly crystalline iron oxyhydrosulfate mineral with a variable composition, typically represented as $Fe_8O_8(OH)_{8-2x}(SO_4)_x$ (x~1-1.75). It naturally occurs in acid mine drainage and is known to be an effective scavenger of arsenate,

fluoride and heavy metals.[13-16] Schwertmannite can be synthesized by adding ferric chloride/nitrate to sodium/potassium sulfate solutions or via H_2O_2 oxidation of $FeSO_4$ solution, while it usually appears as very fine particle, or required to be dialyzed in cellulose membranes over about 30 d and then freeze-dried.[17] Biosynthesis of schwertmannite by *A. ferrooxidans* has been conducted and proved to be an efficient and green preparation approach within short reaction time.[18] *A. ferrooxidans*, is a gram-negative chemolithotrophic acidophilic bacterium, characterized by non-sporulating, rods, 0.5-0.6 um wide by 1.0-2.0 um long, with rounded ends.[19] Abiotic oxidation of ferrous iron is very slow at pH lower than 4, but acidophilic bacteria such as *A. ferrooxidans* can speed up this process by 10^5-10^6 times.[20] *A. ferrooxidans* oxidation of ferrous iron also precedes the precipitation of Fe(III) as hydroxysulfate minerals. Iron biomineralization is believed to involve bacterial cell surfaces serving as nuclei for initial crystal growth, with exopolysacccharides promoting ferric iron deposition on cell surfaces.[21] The inorganic material in environment could migrate, enrich, transform and form secondary minerals under precise control or be induced by the groups on bacteria surface or metabolites.[22] In biosynthetic process, bacteria not only oxidize ferrous ion to ferric iron, but also dominate the biomineralization process. The biosynthesis method is conducive to the formation of materials with hierarchical structure. In previous, the research mainly focused on the influence of temperature, pH, formation time and monovalent cation on materials,[18,23,24] while the chemical modification effect was neglected in biosynthesis. According to previous research, elemental aluminum plays a pivotal role in traditional adsorbent such as α-Al_2O_3, γ-Al_2O_3, kaolin, etc. Meanwhile, it is also used as the modifier to increase density of the active sites.[25, 26] As for the chloride ion, it would be contributed to the formation of akaganéite (*β*-FeOOH) in ferric iron rich environments, which has a tetragonal structure consisting of double chains of edge-shared octahedra that share corners with adjacent chains to form channels running parallel to the c-axis. It is attracted widely interest in environmental area due to the high surface area and narrow pore size distribution.[27] It can speculate that the

synergistic effect may be achieved when aluminum chloride introduced to the biosynthesis system. Based on the consideration, the effect of aluminum chloride on morphology, structure, crystallinity, thermostability and acid-base property of *A. ferrooxidans* biosynthesized iron based material has been systematic investigated. Furthermore, in order to understand the modification on adsorption, the kinetic, capacity and mechanism of copper/chromium adsorption were evaluated and compared.

2. Experimental

2.1 Biosynthesis of the adsorbent

The acidophilic bacterium *A. ferrooxidans* 23270 used in this study was preserved by the Key Laboratory of Biometallurgy of Ministry of Education, China, which was cultured in 9K medium with 47.3 g/L $FeSO_4 \cdot 7H_2O$ as energy source at 30 □，180 rpm. The composition of the 9K medium was as follows: $(NH_4)_2SO_4$ 3.0 g/L、KC1 0.1 g/L、K_2HPO_4 0.5 g/L、$MgSO_4$ 0.5g/L、$Ca(NO_3)_2$ 0.01 g/L. The medium was adjusted to pH 2.0 with 5% (v/v) H_2SO_4 and autoclaved at 121 ℃ for 15 min. Five percent (v/v) of the cultures of *A. ferrooxidans* were inoculated into the 9K medium and incubated at 30 °C for 5 days. Then, the cultures were filtered through 0.45 um filter paper to remove the precipitate and centrifuged at 12,000 rpm for 20 min to harvest the cells. Cells were washed twice and resuspended in distilled water. The obtained cells were added into 250 mL double distilled water which contained $FeSO_4 \cdot 7H_2O/AlCl_3$ ratio in 15/1, 15/5, 15/10 and 15/15 respectively. The cell density of the biosynthesis system was set at 1.0×10^8/mL, which was determined by microscopic counting. The initial pH of the reaction system was set at 2.0, and it incubated at 30 °C for 6 days at 170 rpm. The precipitate was collected with 0.45 μm filter paper through filtration in the 6th day, washed twice with pH 2.0 ddH_2O (H_2SO_4), and dried at room temperature.

2.2 Adsorption experiment

The adsorption experiment was completed in 50 mL polyethylene centrifuge tubes, which contained 0.05 g adsorbent and 10 mL reaction solution with a background electrolyte of 0.01 M $NaNO_3$. The centrifuge tubes were oscillated on shaker at 170 rpm, 30 °C. After the adsorption, the tubes were centrifuged at 12,000 rpm for 2 min at once to separate the biosynthesized materials. All adsorption experiments were conducted in duplicate.

2.2.1 Effect of pH

The solution pH influenced the adsorption process and capacity. The biosynthesized material with $FeSO_4.7H_2O/AlCl_3$ ratio in 15/5 was used to investigate the effect of pH on adsorption. The initial Cu(II)/Cr(VI) concentration was set at 250 mg/L, and the pH of the solution was adjusted to 3, 4, 5, 6, 7 and 8 respectively with 0.1 M NaOH and 5% (v/v) H_2SO_4.

2.2.2 Adsorption kinetic and isotherms

The material formed with $FeSO_4{\cdot}7H_2O/AlCl_3$ ratio in 20/0.1 and 20/5.0 was applied in kinetic study. The initial Cu(II)/Cr(VI) concentration was 250 mg/L, and pH was adjusted to gradient 3.0 and 8.0. Each150 uL supernatant was extracted from the tubes at 1, 3, 7, 15, 30, 60, 90, 120, 180 min.

The initial concentration of Cu(II) or Cr(VI) was 30, 80, 150, 250 and 350 mg/L in single metal adsorption isotherms study. In competitive adsorption experiment with binary metals, the concentration gradient of Cu(II) and Cr(VI) was set at 20, 40, 80, 120 and 160mg/L. The metal retained in adsorbent phase (qt, mg g−1) was calculated by the follow equation:

$$q_t = \frac{(C_0 - C_t)V}{W}$$

Where C_0 (mg L^{-1}) is initial metal concentration, and C_t (mg L^{-1}) is the concentration at time t (min), V (L) is volume of solution and W (g) is weight of adsorbent. The adsorption experiment repeated 2 times, the data averaged.

2.2.3 Materials regeneration

The adsorption–desorption cycles were repeated consecutively 4 times to determine the reusability of sorbents. After the adsorption experiments (250 mg/L), the Cu(II) or Cr(VI) retained adsorbent was centrifuged at 1,000 rpm for 2 min, washed twice for 2 hours (170 rpm) with pH 2.0 deionized water (H_2SO_4).

2.3 Characterization and analytical method

pH values of reaction solutions were determined by using a pHS-3C model digital pH-meter. Scanning electron microscope analyses were performed with FEI Nova NanoSEM 230. The diffuse reflectance infrared fourier transform spectra were conducted on a IRAffinity-1 Fourier Transform spectrometer. Thermal analyses (TG/DSC) were performed on a DSC 200 F3 Maia apparatus. The carrier gas argon 20 was flowed at 110 mL/min. The XPS characterization was conducted with ESCALAB 250Xi Thermo Fisher X-ray Photoelectron. The concentration of Cu(II) and Cr(VI) was detected by spectrophotometry following the following the Bis-(cyclohexanone) oxalyldihydra zone and 1,5-diphenyl-carbazide method respectively.

3. Results and discussion

3.1 Characterization of the modified biogenic materials

3.1.1 SEM and EDS analysis

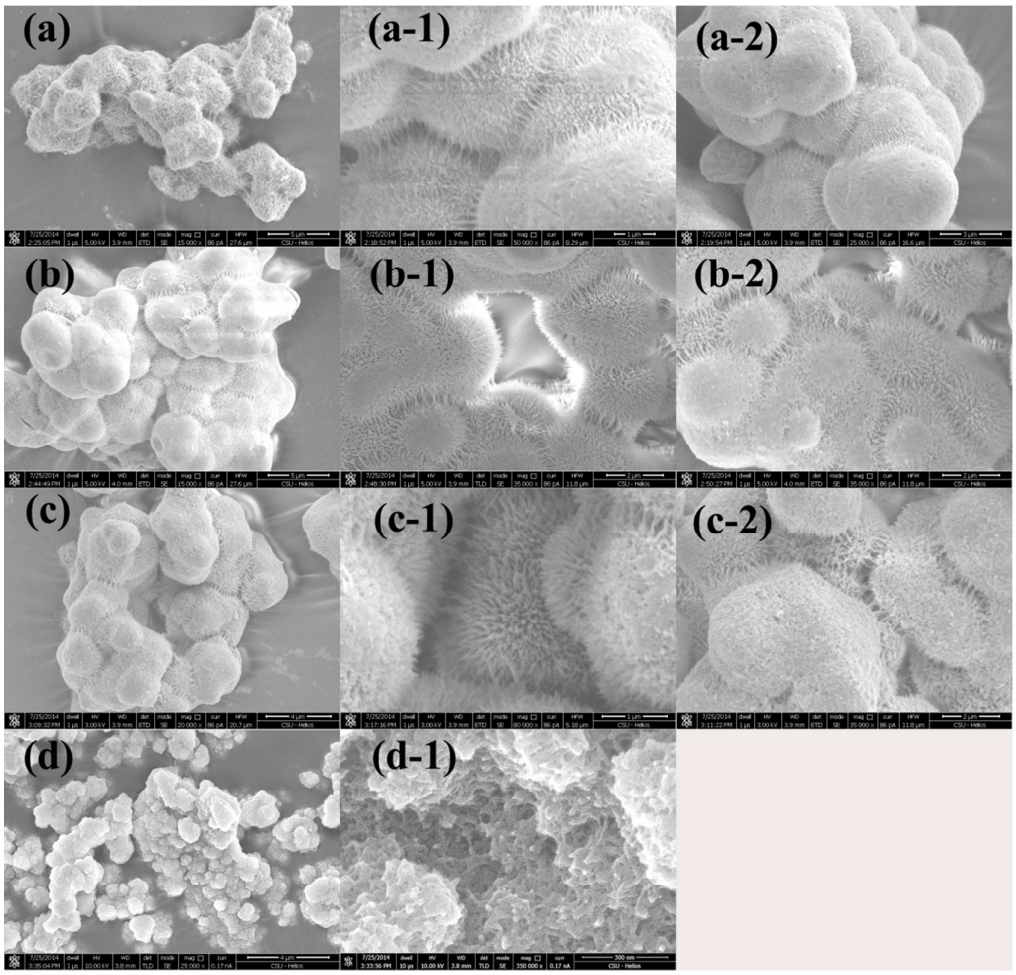

Fig. 1. SEM images of the biosynthesized iron-based materials with different substrate ratio. (a, a-1), (b, b-1), (c, c-1) and (d, d-1) represent the biosynthesized iron-based materials with $FeSO_4 \cdot 7H_2O/AlCl_3$ in 15/1, 15/5, 15/10 and 15/15 respectively. (a-2), (b-2) and (c-2) represent the corresponding material after five consecutive adsorption-desorption cycles.

Fig. 1 showed that the surface morphology and textural property of the modified Schwertmannite varied with ferrous sulfate and aluminum chloride ratio. Fig. 1 (a, a-1) presented the adsorbent formed with $FeSO_4 \cdot 7H_2O/AlCl_3$ ratio in 15/1, which existed as approximately 2 μm diameter spherical aggregates with nanoscale villus covered on the surface. With $FeSO_4 \cdot 7H_2O/AlCl_3$ ratio increased to 20/10, the materials maintained as pompon-like structure. Nanoscale villus on surface became more intensive, while the change of sphere diameter was not significant, maintained about 2 um. When $FeSO_4 \cdot 7H_2O/AlCl_3$ ratio reached 15/15, its villus structure vanished and transformed to rodlike structure, implying the phase transformation with modifier

increasing. The morphology and structure variation showed that aluminum chloride has a significant influence on the biosynthesized iron-based materials. According to previous researches, akaganèite ($FeO(OH)_{1-x}Cl_x$) has a special structure in which four double chains of $FeO_3(OH)_3$ octahedra form a tunnel partly occupied by 1-9 wt% of Cl^-. Schwertmannite has a tunnel structure, akin to that of akaganèite, occupied by SO_4^{2-} that is suggested to share oxygen with two adjacent Fe-chains in the tunnels, which leads to distortion in the structure and the poor crystalloid.[28] When chloride introduced to the biosynthesis system, it may facilitate the akaganèite phase occurrence. Elements composition of the modified biosynthetic materials was shown in Table 1. The surface carbon content changed from 8.69% to 29.04 %, indicated cells or its metabolite adsorbed, served as nuclei for the initial crystal growth and biomineralization process.[21] Aluminum showed a steady increasing trend along with $AlCl_3$ addition, implied aluminum ion play a pivotal role in surface morphology shape process.

Table. 1 Elements composition of the biosynthesized materials.

Fe/Al	C	O	Al	S	Cl	Fe
15:1	28.18	46.84	/	3.03	/	19.75
15:5	8.69	43.25	0.18	5.42	0.34	39.99
15:10	19	40.73	2.12	5.07	0.31	32.14
15:15	29.04	34.80	4.17	4.10	0.25	27.35

3.1.2 XRD, potentiometric titrations

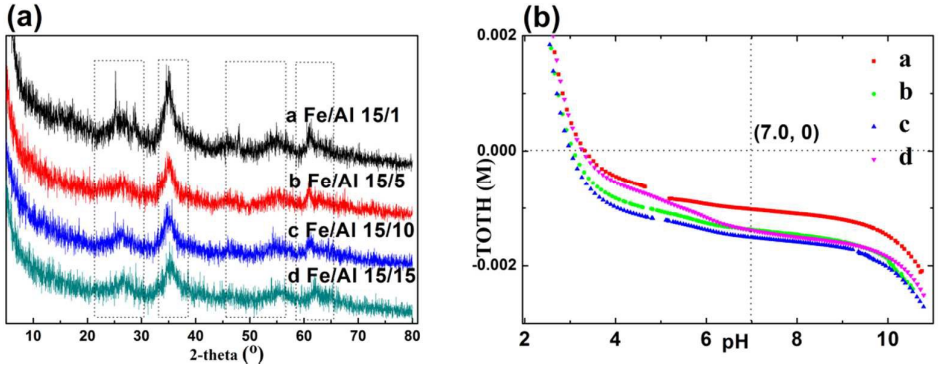

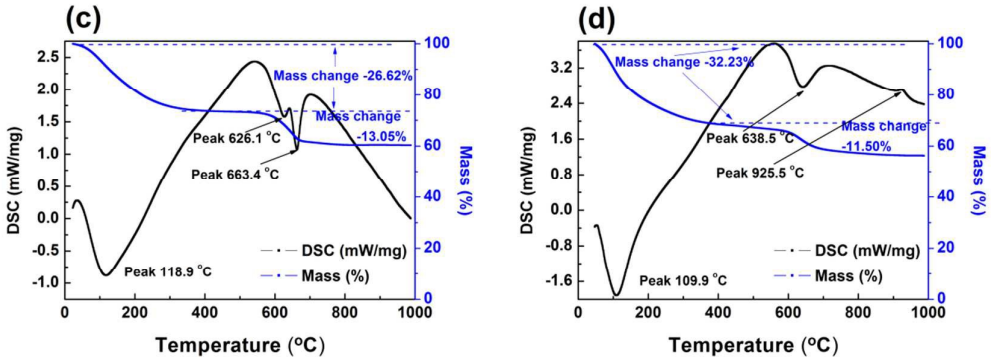

Fig. 2. XRD patterns (a), potentiometric titrations curve (b), and the TG/DSC curve of the formed iron-based materials with $FeSO_4 \cdot 7H_2O/AlCl_3$ in 15/1 (c) and 15/15 (d).

Fig. 2 (a) showed the XRD pattern of materials with different $FeSO_4 \cdot 7H_2O/AlCl_3$ ratio. No sharp, intense peaks can be searched on patterns, illustrating that the formed iron materials are amorphous body. Patterns from a to c exhibited identical characteristic peaks with that of Schwertmannite (PDF 47-1775), and the peak intensity showed a slightly decrease trend. It should noticed the fact that aluminum ion embedded into the Schwertmannite and facilitated the decline in crystallinity.

The adsorption sites concentrations on mineral surface can be determined by potentiometric titrations.[29, 30] The total proton concentration is calculated from the following equation (1):

$$\mathrm{TOTH} = (C_a V_a - C_b V_b)/(V_o + V_a + V_b) \quad (1)$$

Where C_a and C_b are the respective molar concentrations of the HNO_3 and NaOH used, V_o is the initial volume of the suspension, and V_a and V_b are the volumes of HNO_3 and NaOH added. The titration curves (Fig. 2(b)) displayed the heterogeneity in buffering capacity of materials biosynthesized with different substrate ratio. The total proton consumed of the material ($FeSO_4 \cdot 7H_2O/AlCl_3$~15/1-15/15) was -0.00102, -0.00138, -0.00151, -0.00139 M respectively with pH titrating from 2 to 7. The buffering capacity was following the order of $FeSO_4 \cdot 7H_2O/AlCl_3$ ratio in [15/1]<[15/15]≈[15/5]<[15/10]. Functional groups on minerals are the basic units of surface complexation reactions.[30, 31] The deprotonation of a functional group can be represented by the generic reaction (2), where R is the mineral and A represents a functional group on adsorbent. Metal complexation with the deprotonated (x=0) or

protonated (x=1) forms of the monoprotic acids can be expressed as reaction (3), where M^{m+} is the aqueous metal cation. Based on this speculation, it can be speculated that the mechanism of Cu^{2+} and $HCrO_4^{2-}$ adsorption can be expressed as the reaction (4, 5).

$$\mathrm{R-AH^0 \leftrightarrow R-A^- + H^+} \quad (2)$$

$$M^{m+} + R - \mathrm{AH}_x^{(x-1)} \leftrightarrow \mathrm{R-AH}_x(\mathrm{M})^{m+(x-1)} \quad (3)$$

$$\equiv \mathrm{FeOH} + \mathrm{Cu^{2+}} \leftrightarrow \equiv \mathrm{FeO}Cu^+ + H^+ \quad (4)$$

$$\equiv \mathrm{Fe-OH} + HCrO_4^- \leftrightarrow \equiv Fe - OHCrO_4^{2-} + H^+ \quad (5)$$

The TG/DSC curve of the adsorbent biosynthesized with $FeSO_4 \cdot 7H_2O/AlCl_3$ ratio in 15/1 and 15/15 were exhibited in Fig. 2 (c, d). Both materials exhibited similar weight loss process, which can be divided into two stages, the first stage reached 26.62% and 32.23% for $FeSO_4.7H_2O/AlCl_3$ in 15/1 (c) and 15/15 (d) respectively, then followed by 13.05% and 11.50% loss. The first endothermic peak emerged at 118.9 and 109.9 °C in DSC curves was due to the loss of adsorbed water. The next endothermic peaks were observed at 663.4 and 638.5 °C, and accompanied dramatic weight loss, which were caused by thermal decomposition of yavapaiite-type structures. The TG/DSC curves revealed that the material maintained well thermostability after the chemical modification.

3.1.3. FTIR analysis

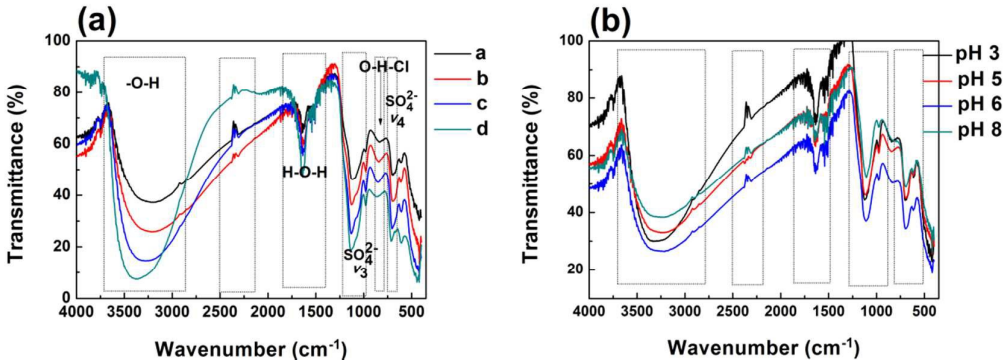

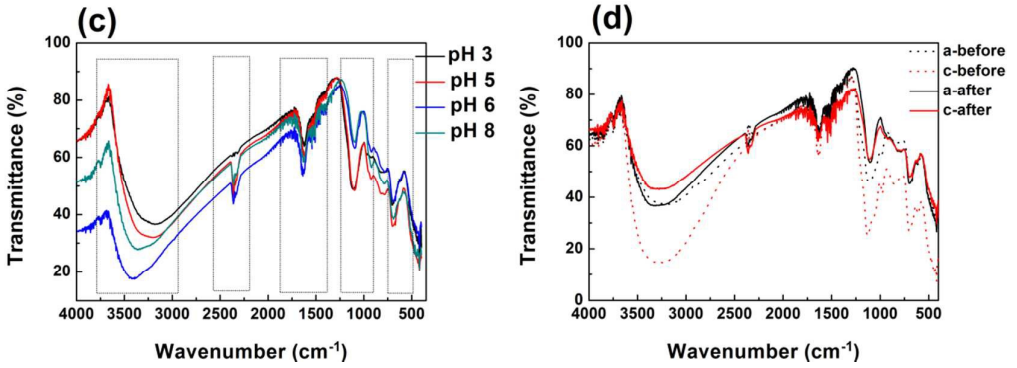

Fig. 3. The FTIR spectra of the materials before and after adsorption. (a) represents the modified materials before adsorption; (b) and (c) represent the material formed with $FeSO_4 \cdot 7H_2O/AlCl_3$ ratio in 15/5 after Cu(II) and Cr(VI) adsorption in different pH; (d) represents materials $FeSO_4 \cdot 7H_2O/AlCl_3$ ratio in 15/1 and 15/10 before and after adsorption respectively.

Fig. 3(a) showed the FTIR spectra of the materials before adsorption, which have similar group composition. The intense broadband observed in the region 2900 to 3700 cm^{-1} can be attributed to O-H stretching (ν_{OH}), and the successive bands of the H-O-H deformation located around 1630 cm^{-1}. A splitting fundamental band at 1136 cm^{-1}, and absorption band around 707 cm^{-1}were caused by ν_3 and ν_4 vibration mode of the sulfate. The bands observed near 607 and 450 cm^{-1} are vibrations of FeO_6 coordination octahedral. The band at 840 cm^{-1} was the vibrating modes of O-H-Cl hydrogen bonds, representative characteristics of Cl containing akaganèite. The whole spectra were basically identical with the spectrum of Schwertmannite, which was confirmed by O-H stretching, H-O-H deformation, ν_3 and ν_4 vibration mode of SO_4^{2-}, and FeO_6 coordination octahedral. While the appearance of representative characteristic O-H-Cl hydrogen bonds illustrated that chloride was incorporated into the Schwertmannite structure after the $AlCl_3$ modification. Furthermore, it should be noticed the fact that the functional group density on Schwertmannite were steady increased with $AlCl_3$ increasing, which were reflected on –O-H, SO_4^{2-} and O-H-Cl absorption intensity. The results of FTIR analysis revealed that the modification effectively enhanced the critical functional group density of the adsorbent.

3.2 Effect of pH on Cu(II) and Cr(VI) adsorption

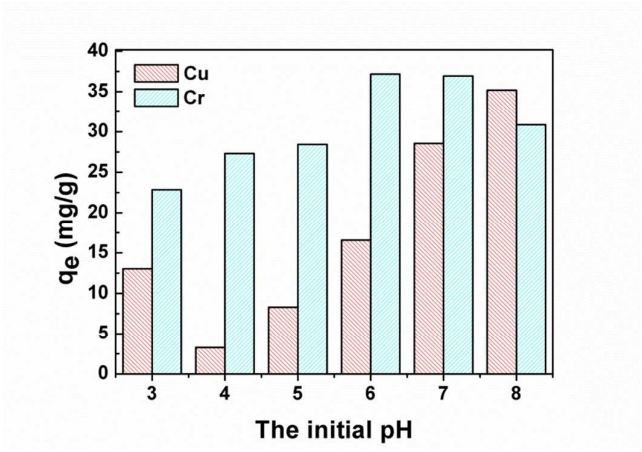

Fig. 4 Effect of solution pH on Cu(II) and Cr(VI) adsorption

The pH of the system controls the adsorption behavior and capacity due to its influence on surface property of the adsorbent and the ionic form of heavy metals. As shown in Fig. 4, the adsorption of Cu(II) increase with pH rising from 4-8, and it reached 35.20 mg/g in pH 8. In lower pH, functional groups such as hydroxyl and sulfate are in protonated cationic forms, repelling the positively charged copper ions and leading to decrease in adsorption. Similarly, the adsorption of Cr(VI) showed an increasing trend between pH 3 and 6, and the maximum adsorption reached 37.18 mg/g in pH 6. The removal efficiency of Cr(VI) in pH 7 and 8 is inferior to that in pH 6. In lower pH environment, protons in solution compete with Cu(II) and Cr(VI) for the bonding sites on adsorbent.[32, 33] $Cr_2O_7^{2-}$, $HCrO_4^-$ or CrO_4^{2-} were co-existed in pH 6.0, and $HCrO_4^-$ existed as the dominant form.[34, 35] $HCrO_4^-$ possess greater affinity toward the proton on the surface, this specific pH environment favored the adsorption process. When pH higher than 7.0, the active sites and chromium ion are in extremely negatively charged state. If chromium and functional groups in mutually repelling state, it lead to the decrease in adsorption capacity. In the optimal pH condition, the highest electrostatic attraction or exchange efficiency with hydroxyl was existed between the adsorbent surface and heavy metals.

3.3 Adsorption kinetics

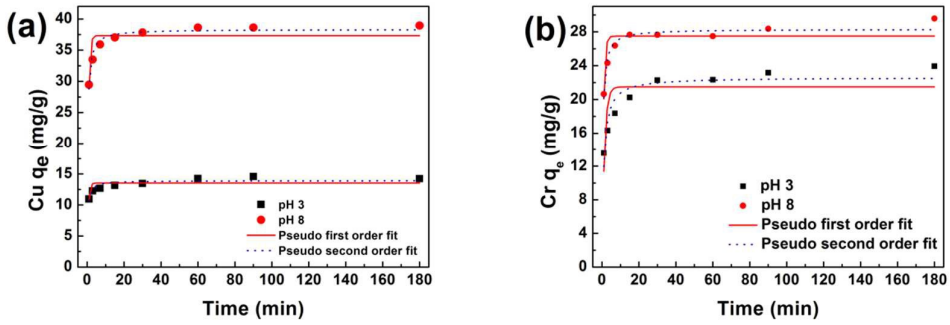

Fig. 5. Adsorption kinetic plots of copper (a) and chromium (b) of schwertmannite biosynthesized with $FeSO_4.7H_2O/AlCl_3$ ratio in 15/5.

Three different kinetic models, the pseudo-first-order, pseudo-second-order and the intraparticle diffusion model, are used to fit the adsorption processes. Kinetic data for Cu(II) and Cr(VI) adsorption are shown in Fig. 4 (a, b). Preliminary investigations on the uptake rate on schwertmannite indicated that the process is rapid. For copper adsorption in pH 8 (Fig. 4(a)), it mainly concentrated on the first 10 minutes and reached about 36 mg/g. After the first-step contacting, it tend to achieve equilibrium gradually (37.3 mg/g). Similarly, for Cr(VI) in pH 8, the rapid reacting appeared in the first 15 minutes, reached 27.66 mg/g. The subsequently adsorption increased about 2 mg/g. The kinetics data was fitted using different models in order to elucidate the sorption mechanism. Initially, the Langergren's pseudo-first-order equation, and pseudo-second-order equation were tested to fit the experimental data. The mathematical representations of the two models are given in Equations (6) and (7), respectively.

$$\ln(q_e - q_t) = \ln q_e - k_1 t \qquad (6)$$

$$\frac{t}{q_t} = \frac{1}{k_2 q_e^2} + \frac{t}{q_e} \qquad (7)$$

Where q_e and q_t ($mg \cdot g^{-1}$) are the amount of adsorbed metals on Schwertmannite at equilibrium and time t, respectively. k_1 is the first order rate constant (min^{-1}). k_2 (mg g^{-1} min^{-1}) is the rate constant of pseudo-second-order. The kinetics parameters of pseudo-first-order and pseudo-second-order were summarized in Table 2. Higher correlation coefficients were observed in the pseudo-second-order model than that of

the pseudo-first-order model (Table 1) for both metals (0.80/0.51 0.95/0.67 0.87/0.57 0.94/0.41). Moreover, the Langergren's pseudo-first-order equation did not give satisfactory fits throughout the range of contact time. The best fits over the entire time range were found with the pseudo-second-order model, indicating chemical adsorption of Cr(VI) and Cu(II) onto the active sites of schwertmannite. The adsorption for Cr(VI) was 22.61 mg/g (pH 3) and 28.31 mg/g (pH 8) respectively. While the Cu(II) adsorption were 13.91 mg/g and 38.33 mg/g. It reconfirmed that the pH dependency for Cr(VI) is weaker than that of Cu(II).

Table. 2 Rate constants calculated based on pseudo-first-order, pseudo-second-order models.

	Lagergren-first-order kinetic model			Pseudo-second-order kinetic model		
	q_e (mg g^{-1})	k_1 (min^{-1})	R^2	q_e (mg g^{-1})	k_2 (mg g^{-1} min^{-1})	R^2
Cu pH3	13.54	1.60	0.51	13.91	0.23	0.80
Cu pH8	37.33	1.49	0.69	38.33	0.08	0.95
Cr pH3	21.49	0.76	0.57	22.61	0.05	0.87
Cr pH8	27.49	1.31	0.71	28.31	0.09	0.94

The pseudo-second-order equation describes the kinetics data as a generalized, one rate-controlling step removal process. However, the intraparticle diffusion model may provide a more comprehensive view of adsorption as a series of distinct steps.[36] In order to understand the differences of kinetic behavior, intraparticle diffusion was investigated using the Weber Morris equation (Equation (8)).

$$q_t = k_i t^{0.5} + c \qquad (8)$$

Where q_e and q_t (mg·g^{-1}) are the amount of adsorbed metals on Schwertmannite at equilibrium and time t, respectively. k_i is the intraparticle diffusion rate constant (mg g^{-1} $min^{-0.5}$). If intraparticle diffusion is the rate-controlling step, then the q_t versus $t^{0.5}$ plot should be linear and pass through the origin. If the plot shows multi-linearity, this indicates further complexity existed in the adsorption process. Multi-linearity was clearly observed in the whole time range in Fig. 6(a, b), showing that two steps governed adsorption rather than one. The adsorption was controlled by two steps or more, including boundary layer or external diffusion, pore diffusion, surface diffusion

and adsorption onto the pore surface or in combination of several steps, of which intraparticle diffusion step was the most limiting procedure. The first stage is the film physical diffusion, which heavy metals transported onto the mineral surface, then it transporting and adsorbing on the interior particle is the second stage. The correlation coefficient of Cr(VI) in second step is pretty higher which means the adsorption can be detached into these two parts of particle diffusion. Also, as reflected in Table 3, the intraparticle diffusion rate constant of Cu(II) in first stage was far higher than that in later stage, which are both observed in pH 3 and 8. It illustrated that the exterior surface adsorption was an instantaneous diffusion process. When exterior surface reached saturation, heavy metal ions entered the mesopores on the second stage with increased diffusion resistance, resulting in the decrease of diffusion rates (k_{i2}).

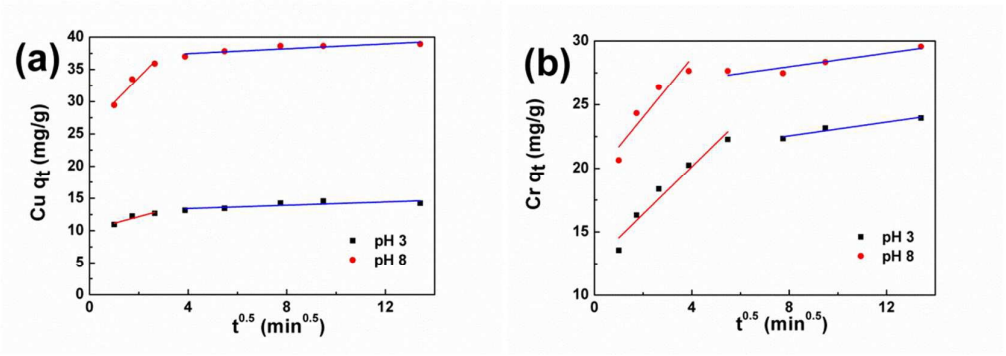

Fig. 6. Plots of intraparticle diffusion model for adsorption of Cu(II) (a) and Cr(VI) (b) of schwertmannite biosynthesized with FeSO4·7H2O/AlCl3 ratio in 15/5.

Table 3 Intraparticle diffusion model for Cu(II) and Cr(VI) adsorption.

	First stage			Second stage		
	c_1 (mg g^{-1})	k_{i1} (mg g^{-1} $min^{-0.5}$)	R^2	c_2 (mg g^{-1})	k_{i2} (mg g^{-1} $min^{-0.5}$)	R^2
Cu pH3	10.14	1.02	0.76	12.92	0.13	0.48
Cu pH8	26.02	3.87	0.92	36.71	0.19	0.72
Cr pH3	12.68	1.86	0.94	20.39	0.27	0.90
Cr pH8	19.37	2.33	0.83	25.87	0.27	0.82

3.4 Equilibrium adsorption isotherms

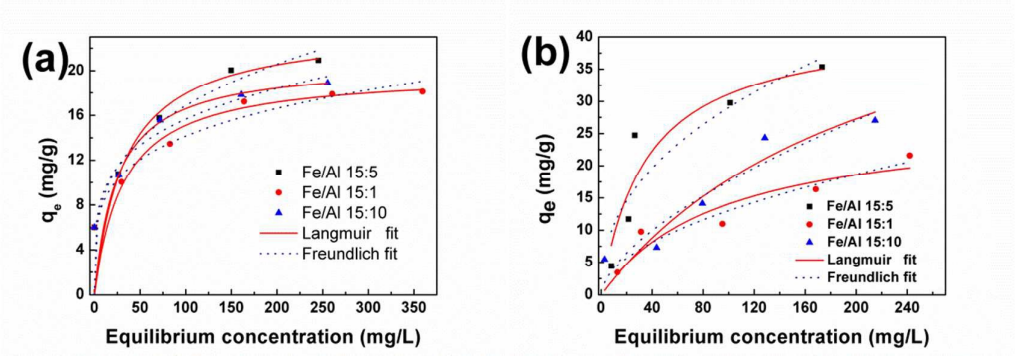

Fig. 7. Langmuir and Freundlich isotherm for Cu(II) (a) and Cr(VI) (b) adsorption.

In order to examine the fundamental adsorption properties regarding interaction and capacity, the equilibrium measurement was performed. The Langmuir (Eq. (9)), Freundlich (Eq. (10)) models are used to fit the experimental data.

$$q = q_m K_L C_e/(1 + C_e) \quad (9)$$

$$q = K_F C_e^{1/n} \quad (10)$$

Where q is the amount of Cr(VI) adsorbed on materials in different concentration; q_m is the saturated adsorption capacity; K_L, a constant of the Langmuir isotherm and C_e is the equilibrium Cr(VI) concentration remained in the solution; K_F is Freundlich constant (L/mg), which indicates the relative adsorption capacity of the adsorbent; n is the heterogeneity factor and is known as Freundlich coefficient. The fitting results are shown in Fig. 7. Table 4 showed that the maximum removal capacity of Cu(II) was in the following order: Schwertmannite biosynthesized with $FeSO_4 \cdot 7H_2O/AlCl_3$ ratio in [15/5](20.95 mg g^{-1})>[15/10](20.72 mg g^{-1})>[15/1](19.90 mg g^{-1}), indicating the active sites and adsorption capacity were enhanced with the modification. However, the promotive effect did not change regularly with the aluminium chloride increasing. Correlation coefficients showed Langmuir model fitted the Cu(II) adsorption data better than the Freundlich model, implying a monolayer adsorption trend. As for the Cr(VI) adsorption, it was promoted from 27.4 mg/g to 57.60 mg/g with $FeSO_4 \cdot 7H_2O/AlCl_3$ ratio increasing. This tendency well illustrated the feasibility of $AlCl_3$ modification in biosynthesis. Freundlich constant (K_F) in Cr(VI) adsorption with $FeSO_4.7H_2O/AlCl_3$ ratio in 15:5 reached 4.04 (Table 4), much higher than others, which indicates the potential in adsorption. The value of 1/n for both Cu(II) and Cr(VI)

lies between 0 and 1 further confirms the favorable adsorption for both metals.

Table 4 The parameters for the Langmuir and Freundlich adsorption isotherms of Cu(II) and Cr(VI)

Fe/Al	Langmuir isotherm			Freundlich isotherm constants constants		
	q_m (mg	K (L m^{-1})	R^2	K_F (mg g^{-1})	n	R^2
15:1	19.90	0.03	0.62	4.85	4.30	0.60
Cu 15:5	23.95	0.03	0.69	4.52	3.49	0.68
15:10	20.72	0.04	0.59	5.35	4.29	0.56
15:1	27.40	0.01	0.85	1.19	1.92	0.91
Cr 15:5	42.26	0.03	0.85	4.04	2.33	0.77
15:10	57.60	0.005	0.86	1.00	1.61	0.86

3.5 Competitive adsorption of Cu(II) and Cr(VI)

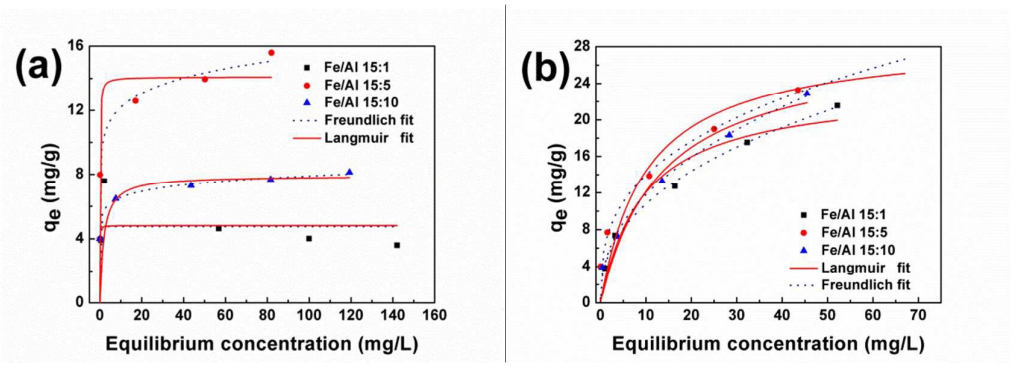

Fig. 8. The Langmuir and Freundlich isotherm for Cu(II) (a) and Cr(VI) (b) competitive adsorption.

Compared with the single metal system, the Cu(II) and Cr(VI) exhibited distinct adsorption behavior in the binary metals system (Fig. 8). In single metal systems, the Cu(II)/Cr(VI) adsorption capacity of each adsorbent (with $AlCl_3$ content increasing) were 19.90/27.40, 23.95/42.26 and 20.72/57.60 (initial concentration 30-450 mg/L), while the adsorption capacity in binary metals system (Table 5) were 4.81/23.63, 14.10/28.89 and 7.92/28.25 (initial concentration 20-160 mg/L). Both Cu(II) and Cr(VI) were completely removed in the second sample added system when the initial concentration was 20 mg/L, which illustrated the depth removal capacity of the modified adsorbent. The correlation coefficients for both Freundlich and Langmuir

model in Cr(VI) adsorption were both higher than that in the single metal system, while the Cu(II) correlation coefficients were remarkable decreased even in negative. This result demonstrated that the modified materials provided more active sites or greater affinity for Cr(VI) in binary metals system. The modification process effectively promoted the adsorption capacity of the adsorbent in binary metals system.

Table 5 The Langmuir and Freundlich parameters of competitive adsorption isotherms of Cu(II) and Cr(VI).

		Langmuir isotherm constants			Freundlich isotherm constants		
	Fe/Al	q_m (mg g^{-1})	K(L mg^{-1})	R^2	K_F (mg g^{-1})	n	R^2
Cu	15:1	4.81	39.00	-0.32	4.75	1.47E+24	-0.33
	15:5	14.10	10.88	0.70	9.68	9.95	0.76
	15:10	7.92	0.56	-1.02	5.45	12.45	-1.00
Cr	15:1	23.63	0.10	0.92	4.14	2.41	1.00
	15:5	28.89	0.10	0.88	6.36	2.93	0.95
	15:10	28.25	0.08	0.93	4.37	2.32	0.99

3.6 Influence of co-existing anions and materials regeneration on adsorption

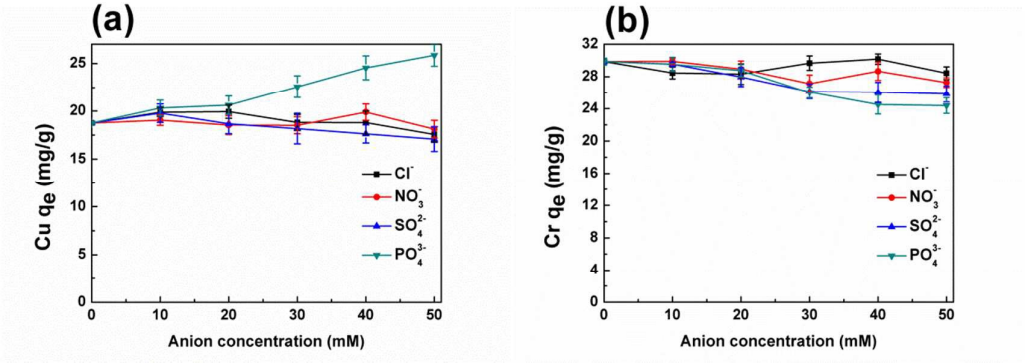

Fig. 9. Adsorption capacity of Cu(II) (a) and Cr(VI) (b) in presence of co-existing anions..

Co-existing anions in wastewater influenced the heavy metals adsorption behavior and capacity. As shown in Fig. 9(a, b), anions NO_3^-, Cl^-, SO_4^{2-}, and PO_4^{3-} have diverse impacts on the adsorption. The influence of NO_3^- and Cl^- on both metals was not significant. The removal efficiency maintained higher than 90% with anion concentration increasing. As for the sulfate, it led to the adsorption decreased from

18.75 to 17.08 mg/g. When sulfate introduced to the system, $\equiv FeSO_4^-$ or $\equiv FeOHSO_4^{2-}$ would be formed on Schwertmannite surface,[37] which competed for Cu(II) adsorption active sites, and inhibited the adsorption. Phosphate in the system remarkably enhanced the Cu(II) adsorption capacity to 25.85 mg/g with the concentration increasing. As revealed in Fig. 4, Cu(II) adsorption was highly pH depended, the buffer ability of phosphate maybe contributed to maintain a higher pH environment. Both SO_4^{2-} and PO_4^{3-} showed inhibition effect especially for $Cr_2O_7^{2-}$ in higher concentration. The previous research showed oxyanions on metals adsorption follow the selectivity order $Cl^- < NO_3^- < SO_4^{2-} < HPO_4^{3-}$ on analogous mineral akaganeite.[38] Anions especially oxyanions competed for active sites on adsorbent, which resulted in the decreasing in adsorption.

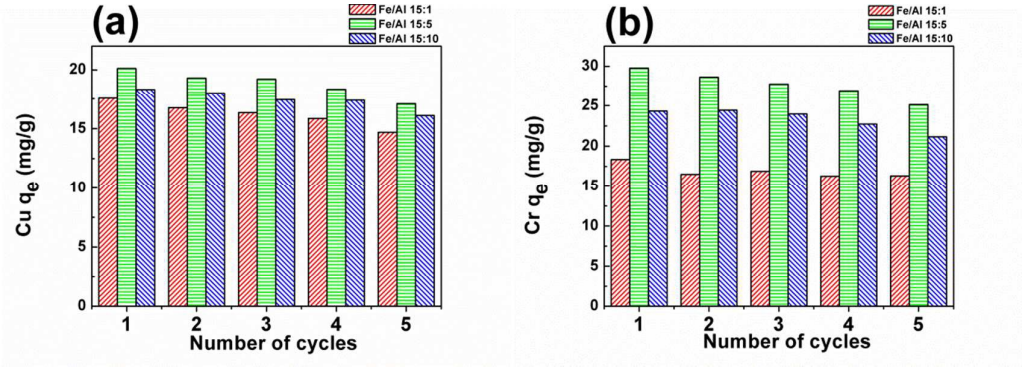

Fig. 10. Adsorption capacity of regenerated adsorbent for five consecutive cycles.

To evaluate the recyclability of the modified biosynthetic adsorbent, a five successive adsorption–desorption cycles experiment were performed. Metals on Schwertmannite were desorbed with pH 2.0 (H_2SO_4) deionized water washing. It can be identified from Fig. 10 that the adsorption capacity of the regenerated materials were slightly decreased, while it was maintained in an acceptable scope. The microstructure change (Fig. 2 a-2, b-2, c-2) showed that part of the surface covered nanoscale villus vanished after five consecutive cycles, while the whole structure remained intact. It explained the slightly decline in adsorption capacity with the adsorption-desorption cycles. At the end cycles, the materials retained more than 80% of its original adsorption capacity for both metals. It demonstrated that the active sites can be regenerated by pH 2.0 water washing, giving rise to the practical application potential in the

treatment of heavy metal contaminated wastewater.

3.7 Adsorption mechanism

3.7.1. Correlation between released H^+ and adsorption capacity

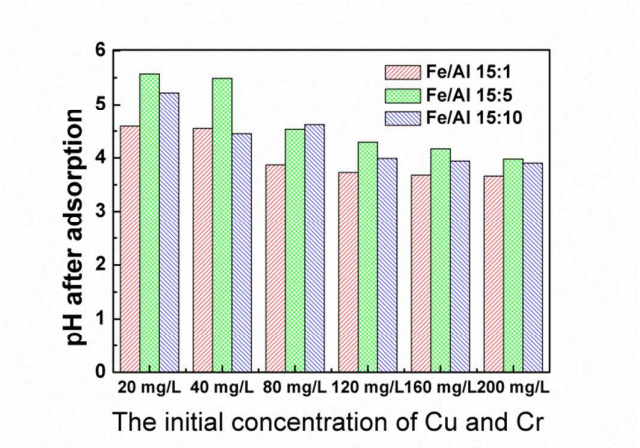

Fig 11. Solution pH after adsorption in binary metals system.

Fig 11 showed the pH in the binary metals system gradient declined after adsorption. The decline extent of material formed with $FeSO_4 \cdot 7H_2O/AlCl_3$ in 15/1 was higher than that of $FeSO_4 \cdot 7H_2O/AlCl_3$ in 15/10, and then followed by that in 15/5, which was negatively related with the adsorption capacity. Noticed the content of hydroxyl group declined obviously (Fig. 3), it can speculate heavy metals may participate in cation exchange with hydrogen ions on adsorbent surface.

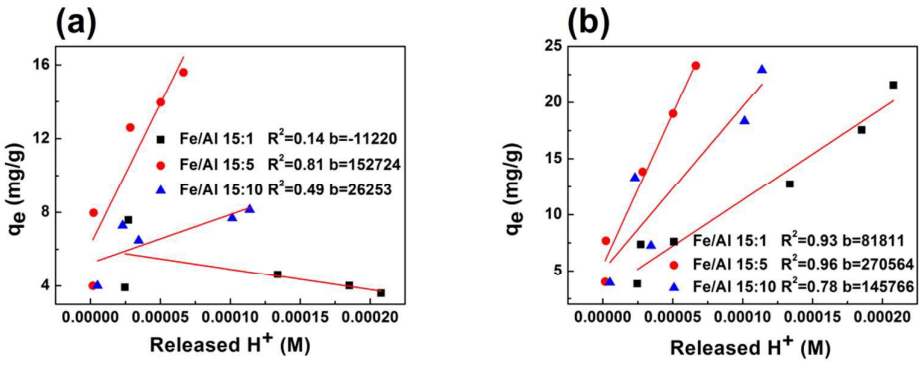

Fig. 12. The correlation between the released H^+ and adsorbed metals Cu(II) (a), Cr(VI) (b).

Fig. 12 showed the linear fitting model between the released H^+ and adsorbed metals. It revealed the correlation between released H^+ and adsorption capacity. As for the

Cr(VI) adsorption, it exhibited a positive linear relationship with the released H^+, which reached 0.93, 0.96, and 0.78 respectively, while the fitting degree of Cu(II) was only 0.14, 0.81, and 0.49. The fitting degree showed the adsorbent possess higher affinity for Cr(VI) in binary system. The fitting linear slope of material formed with $FeSO_4.7H_2O/AlCl_3$ in 15/5 reached 152724 and 270564 for Cu and Cr respectively, higher than the rest materials, implying it possess much higher exchange efficiency in this modification ratio.

1.7.2. FTIR spectra after adsorption

FTIR spectra of the materials before and after adsorption were presented in Fig. 3 (a, b, c, d). The adsorption intensity of hydroxyl group (2900 to 3700 cm^{-1}) obviously reduced after adsorption, which reconfirmed the correlation between the released H^+ and adsorbed metals, and the critical role of –O-H was in adsorption (Equation (4, 5)). Electrovalent coordination bond would be formed between the functional groups and heavy metals on adsorbent. However, reduce in intensity of hydroxyl group (Fig. 3 b, c) was not always consistent with the adsorption capacity, revealed hydroxyl was not the only group involved in adsorption. At a lower pH, the system produces more competition for adsorption sites between metals and the increased hydrogen ion. Additionally, the intensity of O-H-Cl and SO_4^{2-} also declined (Fig. 3 b, c), which was due to the ligand exchange between metals and Cl^-/SO_4^{2-} on adsorbent. It should be noticed that the decline extent of –O-H and O-H-Cl/SO_4^{2-} varied with metals. Fig. 3(d) showed that, in binary metals system, all groups above reached the most remarkable decline. In sole Cu(II) adsorption, the decline concentrated on -O-H (Fig. 3b), while O-H-Cl/SO_4^{2-} were dominated groups in Cr(VI) adsorption (Fig. 3c), indicating the heterogeneity in adsorption sites between metals.

3.7.3. XPS spectra after adsorption

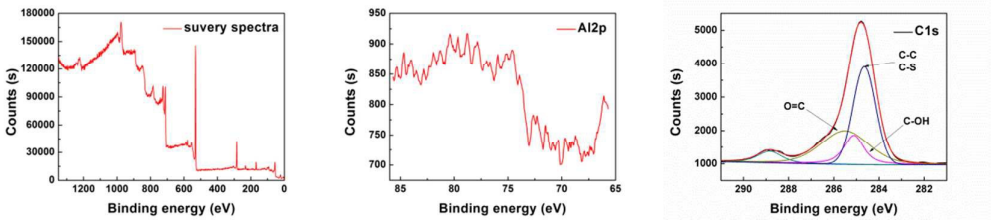

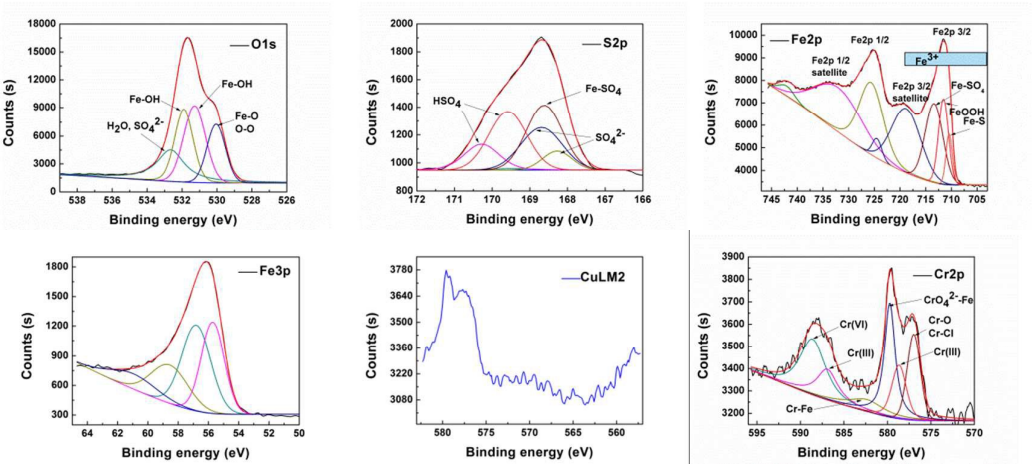

Fig. 13. High-resolution XPS spectra showing fits of the C, Fe, O, S, Al, Cu, Cr. Black lines refer to the experimental spectra, red lines that overlap lines refer to linear combination fitting results.

Table. 6 Surface element composition of the materials after adsorption.

Name	Start BE	Peak BE	End BE	FWHM	Area (P) CPS.eV	Atomic %
C1s	290.79	284.8	282.39	1.44	7790.79	29.19
O1s	535.19	531.6	527.99	2.63	37024.91	51.47
S2p	171.59	168.79	166.79	2.04	1838.53	3.57
Fe2p	739.39	711.42	707.89	3.94	46835.88	13.96
Cr2p1	592.99	588.16	584.19	3.86	1102.42	1.1
Al2s	121.59	119.02	117.19	0.93	154.57	0.7

The XPS spectra of the adsorbents biosynthesized with $FeSO_4 \cdot 7H_2O/AlCl_3$ in 15/5.0 after adsorption are shown in Fig. 13. Table 6 summarized the surface element composition on adsorbent. The residual carbon content reached 29.19% (atomic%), C-C/C-H, C-OH, O=C, N=C-O were identified in the spectra. In biosynthesis, bacteria oxidized ferrous iron, and played as the biosurfactant in inorganic element migrate, enrich, transform and secondary minerals formation. The Fe 2p core levels are split into 2p 3/2 and 2p 1/2 doublets due to the spin–orbit coupling (Fig. 12). Moreover, positions of their satellites are also sensitive to the Fe oxidation and bonding state. All bonding energies of Fe 2p 3/2 lines are higher than 710 eV, which strongly suggests that iron is presented as Fe(III) species. Fitted Fe 2p lines results showed that Fe-SO_4, Fe-S, and FeOOH existed in adsorbent, which played as the structural composition as well as the active sites. This result was further testified by the O 1s and S2p spectra. The peaks at 529.9 and 531.3 eV can be assigned to the lattice oxygen atoms bonding with Fe (Fe-O) and the lattice hydroxyl (Fe-OH lattice),

respectively, which served as the active sites in adsorption. As for the state of chromium, the surface content reached 1.1%, the peak appeared in higher bonding energy 588.6 and 579.8 eV can be assigned to Cr(VI) forms characterized as CrO_4^{2-}, while the peak in 586.89 and 578.69 were regarded as Cr(III) compounds. The existing of Cr(III) on adsorbent surface illustrated that Cr(VI) could be reduced to the less toxicity form Cr(III) by the biosynthesized mineral, which may be reduction through the photo-reduction way. Furthermore, the peak located in 579.8 eV can be assigned CrO_4^{2-} group bonding with Fe, the Cr-Fe bonding structure was also observed in 583.0 eV locations. The peak appeared in 576.99 eV was the characteristic peak of lattice oxygen or chloride atoms bonding with Cr. The atoms bonding structure in XPS spectra reconfirmed the adsorption mechanism. Based on the analysis above, Schematic of the modification effect and the adsorption mechanism were summarized in Fig. 14.

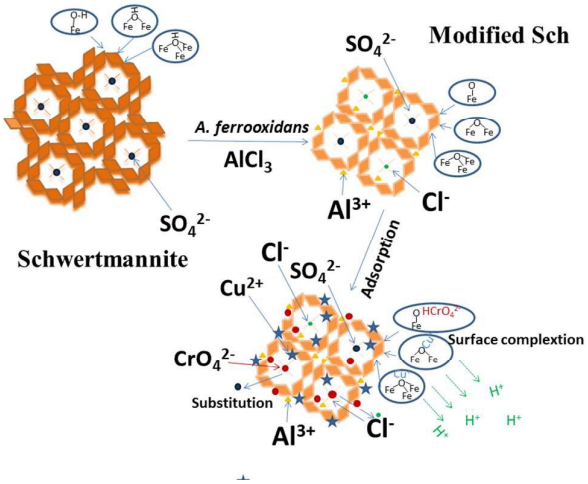

Fig. 14. Schematic of the modification effect and the adsorption mechanism.

4 Conclusions

The results of the present study demonstrate that aluminum chloride modified Schwertmannite were successfully biosynthesized by *Acidithiobacillus ferrooxidans*. With $AlCl_3$ increase, the biosynthesized material transformed from nanoscale villus covered spherical aggregates to rodlike structure consisting globe, and it facilitated

akaganèite analogue transformation and crystallinity decreasing. The optimum pH for Cr(VI) adsorption was maintained between 6.0-7.0, while the adsorption capacity for Cu(II) was increased over pH range 4.0-8.0. Adsorption kinetic varied with pH and adsorbents. The adsorption equilibrium reached within 30 min for both metals. The best fits over the entire time range were found with the pseudo-second-order model. The maximum Cu(II) adsorption capacity was 23.95 mg/g when $FeSO_4.7H_2O/AlCl_3$ ratio in 15:5, while Cr(VI) reached 57.60 with $FeSO_4.7H_2O/AlCl_3$ ratio in 15:10. As for the binary metals system, the maximum adsorption for Cu(II) and Cr(VI) reached 14.10 and 28.89 mg/g respectively, achieved in $FeSO_4.7H_2O/AlCl_3$ ratio in 15:5. The modification enhanced the Cr(VI) selectively adsorption capacity in binary metals system. The biosynthesized materials could be effectively regenerated through pH 2.0 water washing. FTIR, XPS and released proton correlation analysis revealed that –O-H, O-H-Cl and SO_4^{2-} were the key groups in adsorption. Heavy metals adsorbed on Schwertmannite through cation exchange, and surface complexation. Heavy metals can be effectively removed by the modified biosynthetic Schwertmannite.

Acknowledgements

This research was supported by the National Natural Science Foundation of China (51174239), the Fundamental Research Funds for the Central Universities of Central South University (2015zzts089) and the Hunan provincial Co-Innovation Center for Clean and Efficient Utilization of Strategic Metal Mineral Resources.

References

1. S. K. R. Yadanaparthi, D. Graybill and R. von Wandruszka, *Journal of Hazardous Materials*, 2009, **171**, 1-15.
2. A.-F. Ngomsik, A. Bee, J.-M. Siaugue, D. Talbot, V. Cabuil and G. Cote, *Journal of Hazardous Materials*, 2009, **166**, 1043-1049.
3. M. Gan, S. Zhou, M. Li, J. Zhu, X. Liu and L. Chai, *Environmental Science and Pollution Research*, 2015, **22**, 5807-5816.
4. C. O. Ijagbemi, M.-H. Baek and D.-S. Kim, *Journal of Hazardous Materials*, 2009, **166**, 538-546.
5. F. Pagnanelli, S. Mainelli, L. Bornoroni, D. Dionisi and L. Toro, *Chemosphere*, 2009, **75**,

1028-1034.
6. M. Hua, *J Hazard Mater*, 2012, **211**, 317-331.
7. D. Lin, S. Zhou and P. Xiaoxu, *RSC Advances*, 2015.
8. G. Zeng, Y. Liu, L. Tang, G. Yang, Y. Pang, Y. Zhang, Y. Zhou, Z. Li, M. Li, M. Lai, X. He and Y. He, *Chem Eng J*, 2015, **259**, 153-160.
9. L. Cao, Y. Ni, M. Wang and X. Ma, *RSC Advances*, 2013, **3**, 3585-3591.
10. H.-J. Cui, J.-K. Cai, J.-W. Shi, B. Yuan, C.-L. Ai and M.-L. Fu, *RSC Advances*, 2014, **4**, 10176-10179.
11. G. Ona-Nguema, G. Morin, F. Juillot, G. Calas and G. E. Brown, *Environmental science & technology*, 2005, **39**, 9147-9155.
12. P. Mäkie, G. Westin, P. Persson and L. Osterlund, *The Journal of Physical Chemistry A*, 2011, **115**, 8948-8959.
13. S. Regenspurg and S. Peiffer, *Applied Geochemistry*, 2005, **20**, 1226-1239.
14. A. Eskandarpour, M. S. Onyango, A. Ochieng and S. Asai, *Journal of hazardous materials*, 2008, **152**, 571-579.
15. J. G. Webster, P. J. Swedlund and K. S. Webster, *Environmental Science & Technology*, 1998, **32**, 1361-1368.
16. M. Gan, S. Sun, Z. Zheng, H. Tang, J. Sheng, J. Zhu and X. Liu, *Applied Surface Science*, 2015, **356**, 986-997.
17. S. Regenspurg, A. Brand and S. Peiffer, *Geochim Cosmochim Ac*, 2004, **68**, 1185-1197.
18. Y. Liao, L. Zhou, J. Liang and H. Xiong, *Materials Science and Engineering: C*, 2009, **29**, 211-215.
19. A. B. Jensen and C. Webb, *Process biochemistry*, 1995, **30**, 225-236.
20. M. Wang and L. Zhou, *Hydrometallurgy*, 2012, **125**, 152-156.
21. F. S. Jones, J. M. Bigham, J. P. Gramp and O. H. Tuovinen, *Materials Science and Engineering: C*, 2014, **44**, 391-399.
22. J. Zhu, M. Gan, D. Zhang, Y. Hu and L. Chai, *Materials Science and Engineering: C*, 2013, **33**, 2679-2685.
23. J. O. Claassen and R. Sandenbergh, *Hydrometallurgy*, 2007, **86**, 178-190.
24. J. P. Gramp, F. S. Jones, J. M. Bigham and O. H. Tuovinen, *Hydrometallurgy*, 2008, **94**, 29-33.
25. Y. Nie, C. Hu and C. Kong, *J Hazard Mater*, 2012, **233**, 194-199.
26. M. Barathi, A. S. K. Kumar, C. U. Kumar and N. Rajesh, *RSC Advances*, 2014, **4**, 53711-53721.
27. H. Xiong, Y. Liao and L. Zhou, *Environmental science & technology*, 2008, **42**, 8681-8686.
28. H. Xiong, Y. Liao, L. Zhou, Y. Xu and S. Wang, *Environ Sci Technol*, 2008, **42**, 4165-4169.
29. L. Fang, P. Cai, P. Li, H. Wu, W. Liang, X. Rong, W. Chen and Q. Huang, *Journal of hazardous materials*, 2010, **181**, 1031-1038.
30. L. Fang, Q. Huang, X. Wei, W. Liang, X. Rong, W. Chen and P. Cai, *Bioresource Technol*, 2010, **101**, 5774-5779.
31. V. Guine, L. Spadini, G. Sarret, M. Muris, C. Delolme, J. P. Gaudet and J. M. F. Martins, *Environ Sci Technol*, 2006, **40**, 1806-1813.
32. O. Ajouyed, C. Hurel, M. Ammari, L. B. Allal and N. Marmier, *Journal of hazardous materials*, 2010, **174**, 616-622.
33. Y. Zhang, X. Zhao, H. Huang, Z. Li, D. Liu and C. Zhong, *RSC Advances*, 2015.

34. C.-H. Weng, Y. Sharma and S.-H. Chu, *Journal of hazardous materials*, 2008, **155**, 65-75.
35. C. Namasivayam and R. Yamuna, *Chemosphere*, 1995, **30**, 561-578.
36. M. D'Arcy, D. Weiss, M. Bluck and R. Vilar, *Journal of Colloid and Interface Science*, 2011, **364**, 205-212.
37. P. Swedlund and J. Webster, *Applied Geochemistry*, 2001, **16**, 503-511.
38. R. Chitrakar, S. Tezuka, A. Sonoda, K. Sakane, K. Ooi and T. Hirotsu, *Journal of Colloid and Interface Science*, 2006, **298**, 602-608.